HOSTED BY
ELSEVIER
CrossMark
Available online at www.sciencedirect.com
ScienceDirect
Progress in Natural Science: Materials International 25 (2015) 414–418
Progress in Natural Science Materials International
www.elsevier.com/locate/pnsmi
www.sciencedirect.com

Original Research

Microstructural evolution and mechanical behavior of metastable β-type Ti–30Nb–1Mo–4Sn alloy with low modulus and high strength

Shun Guo[a,b,*], Qingkun Meng[b], Xiaonong Cheng[a], Xinqing Zhao[b,**]

[a]Institute for Advanced Materials, Jiangsu University, Zhenjiang 212013, China
[b]School of Materials Science and Engineering, Beihang University, Beijing 100191, China

Received 14 July 2015; accepted 1 August 2015
Available online 29 October 2015

Abstract

A metastable β-type Ti–30Nb–1Mo–4Sn alloy with ultralow elastic modulus and high strength was fabricated. Under the solution treatment state, the Ti–30Nb–1Mo–4Sn alloy possesses low yield strength of about 130 MPa owing to the presence of the coarse α″ martensitic laths. Upon a cold rolling and annealing process, the martensitic transformation from β to α″ is significantly retarded due to the inhibitory effect of grain boundaries and dislocations. As a result, the metastable β phase with low total amount of β-stabilizers is retained to room temperature, giving rise to a low modulus of 45 GPa. Meanwhile, nano-sized α precipitates and dislocation tangles play a key role in strengthening the Ti–30Nb–1Mo–4Sn alloy, resulting in a high tensile strength of ~1000 MPa. With low elastic modulus and high strength, the metastable β-type Ti–30Nb–1Mo–4Sn alloy could be a potential candidate for biomedical materials.

Keywords: Metastable β Ti alloy; β stability; Martensitic transformation; Low modulus; High strength

1. Introduction

As orthopedic implant alloys, commercially pure Ti (C.P. Ti) and Ti–6Al–4V alloy have been widely employed due to their light density, good corrosion resistance, excellent biocompatibility and appropriate mechanical properties [1–3]. However, these alloys have an elastic modulus of ~110 GPa, which is remarkably higher than that of bone tissue (~30 GPa) [1,4]. Such high modulus mismatch can lead to so-called "stress shielding effect" and eventual failure of the implant [5,6]. The motivation to avoid "stress shielding effect" has led to an increasing focus on metastable β-type Ti alloys with lower modulus. In the past decades, various types of metastable β-type Ti alloys have been developed for this purpose, e.g., Ti–Ta [7], Ti–Nb–Ta–Zr [8], Ti–Nb–Ta–Mo [9], etc. However, these alloys possess elastic modulus within the range of 50–80 GPa, still not low enough to match that of bone tissue [1,7–10]. Thus, developing metastable β-type Ti alloys with lower modulus has become an attractive topic in the research and development of advanced biomedical materials.

Previous experimental and computational results have shown that the elastic modulus of β phase is closely related to its total amount of β-stabilizers (e.g. Nb, Ta, Mo, etc.), and decreases monotonically with decreasing total content of β-stabilizers [11–13]. Thus, from the perspective of designing β-type Ti alloys with low modulus, the amount of β-stabilizers in the metastable β-type Ti alloys should be reduced as low as possible. However, when the amount of β-stabilizers is insufficient, the high-temperature β phase will decompose into α′ and/or α″ martensite [14,15]. In this case, the yield strength of the alloys is reduced significantly owing to the occurrence of the stress-induced martensitic transformation [16].

Recent studies revealed that besides the addition of the β-stabilizers, some structural factors induced by a thermo-mechanical process, such as grain refinement and dislocations,

*Corresponding author at: Institute for Advanced Materials, Jiangsu University, Zhenjiang 212013, China.
Tel.: +86 511 88783268; fax: +86 511 88797783.
**Corresponding author. Tel.: +86 10 82338559; fax: +86 10 82338200.
E-mail addresses: shunguo@ujs.edu.cn (S. Guo), xinqing@buaa.edu.cn (X. Zhao).

http://dx.doi.org/10.1016/j.pnsc.2015.09.008

can play a key role in retarding the martensitic transformation of β phase [14,17,18]. This implies that the β phase with less β-stabilizers could be retained to room temperature by the aid of these structural factors. Apparently, this might provide a novel approach of developing β-type Ti alloys with low elastic modulus.

In addition to low elastic modulus, high yield strength is another key demand for implant materials to undertake the complicated cyclic loading [1,10]. However, the yield strength of the current biomedical β-type Ti alloys is commonly much lower than that of conventional Ti–6Al–4V [1,6,10]. Currently, a balanced approach is to strengthen the alloy by α precipitates formed during aging or annealing, at the expense of sacrificing low modulus [19,20]. In such a case, the "stress shielding" problem caused by the elastic modulus mismatch between the implant materials and adjacent bone tissues will be aggravated further. Therefore, it is quite necessary to find out a solution to simultaneously achieve high strength and ultralow modulus in biomedical β-type Ti alloys.

In the present paper, by alloying and thermo-mechanical process, an attempt was made to fabricate a metastable β-type Ti–Nb–Mo–Sn alloy with ultralow modulus and high strength. Based on the combining results from X-ray diffraction, transmission electron microscope, tensile test, dynamic mechanical analyzer and in-situ synchrotron X-ray diffraction, the relationship between microstructural evolution and mechanical properties was discussed.

2. Experimental procedure

A metastable β-type Ti–30Nb–1Mo–4Sn (wt%, hereafter denoted as Ti-3014) alloy was prepared by a vacuum arc melting method using Ti (99.99%), Nb (99.95%), Mo (99.95%) and Sn (99.95%) as raw materials. The arc-melted button was homogenized at 1173 K for 5 h and then hot forged at 1073 K, with the dimensions as follows: 80 mm (length) × 40 mm (width) × 8 mm (thick). The forged ingot was encapsulated in an evacuated quartz tube, solution treated at 1073 K for 1 h and then quenched into water (~298 K). The resultant specimens will be denoted as ST specimens henceforth. After quenching, the ingot was cold rolled into a plate of ~1 mm in thickness, at a thickness reduction of ~88%. The cold rolled plate was annealed at 625 K for 30 min and then quenched into water. The resultant specimens will be referred to CRA specimens hereafter.

Phase constitutions were detected by X-ray diffraction (XRD) analysis with a Cu-Kα irradiation. Uniaxial tensile tests were performed along the rolling direction, using specimens with a rectangular cross-section of $1 \times 1.5\ mm^2$ and a gage length of 30 mm, at an initial strain rate of $1 \times 10^{-3}\ s^{-1}$. In order to ensure the accuracy of strain measurement, an extensometer was employed in the present study. Martensitic transformation start (Ms) temperatures were determined by a dynamic mechanical analyzer (DMA) in a single cantilever mode, using a dynamic stress frequency of 1 Hz and a cooling rate of $5\ K\ min^{-1}$. Microstructure observations and compositional analyses were conducted on a FEI Quanta 200F transmission electron microscope (TEM) equipped with energy dispersive X-ray spectroscopy (EDS) operating at a voltage of 200 kV. In-situ synchrotron X-ray experiments were carried out at room temperature using the 11-ID-C beam-line of Advanced Photon Source (APS) at Argonne National Laboratory (ANL). A monochromatic X-ray beam with a wavelength of 0.10798 Å and a beam size of 0.4 mm × 0.4 mm was employed to obtain two-dimensional (2-D) diffraction patterns during tensile. The 2-D diffraction patterns were processed in Fit2d software and then output one-dimensional (1-D) patterns for analysis.

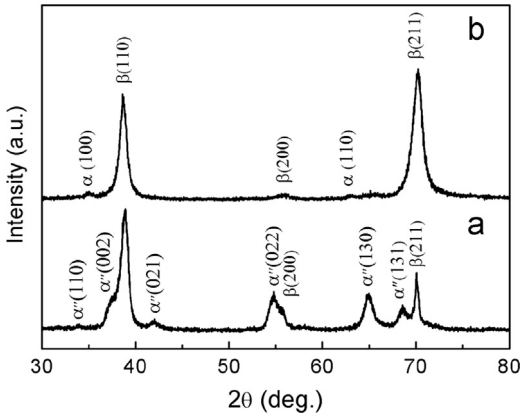

Fig. 1. XRD patterns of ST (a) and CRA (b) Ti-3014 specimens.

3. Results and discussion

Fig. 1(a) and (b) shows the XRD patterns of ST and CRA Ti-3014 specimens, respectively. A mixture of β parent phase and α″ martensite was observed in the ST specimen, indicating that the ST alloy exhibits a martensitic start transformation (Ms) temperature higher than room temperature. This can be ascribed to the low total amount of β-stabilizers in the present alloy. Interestingly, upon a cold rolling plus annealing at 625 K for 30 min, the diffraction peaks ascribed to α″ martensite phase disappeared in the XRD diffraction pattern, as shown in Fig. 1(b). This result suggests that α″ phase formed before annealing was transformed reversibly to β phase during annealing, and in the subsequent cooling process the martensitic transformation from β to α″ did not take place any more. Instead, a few α precipitates was observable in the CRA Ti-3014 alloy, as evidenced by relative weak diffraction peaks of α phase, i.e., α(100) and α(110).

The storage modulus, which can be utilized to determine the Ms temperature from β to α″, was measured by DMA during cooling for the ST and CRA specimens, and the results are shown in Fig. 2. The storage modulus, in both ST state and CRA state, was found to decrease with decreasing temperature and then increase with further decreasing temperature. On the basis of the results shown in Fig. 2, the Ms temperatures of the ST and CRA alloys were determined to be ~339 K and ~226 K, respectively. It should be noted that the Ms temperature for CRA alloy is ~113 K lower than that for ST alloy. This suggests that the martensitic transformation from β to α″ can be remarkably postponed through the simple cold rolling plus annealing process, which is in agreement with the results obtained using the XRD technique.

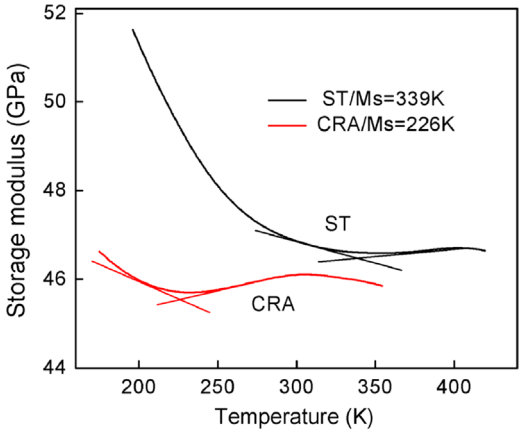

Fig. 2. Storage modulus versus temperature during cooling for ST and CRA Ti-3014 specimens.

Fig. 3 presents a typical bright-field micrograph (a) and the corresponding [110]β zone axis selected area diffraction pattern (SADP) (b) of ST Ti-3014 specimen. In the bright-field image, α″ martensitic laths were visible within the coarse β parent phase. Referring to the SADP shown in Fig. 3(b), one can see that in addition to the primary reflections from β matrix, additional spots ascribed to α″ martensite were visible near the 1/2 {112}β positions. In addition, no extra reflections can be observed at the 1/3 and 2/3 {112}β positions in Fig. 3(b), indicating that athermal ω phase does not form in the ST specimen.

Fig. 4(a) shows the bright-field micrograph of CRA specimen, indicating that upon a cold rolling plus annealing process, the coarse α″ martensitic laths disappeared. Instead, a few nanometer-scale precipitates, labeled with a white arrow in Fig. 4(a), are observable in the CRA specimen. Additionally, some irregular dark areas originating from dislocation tangles were clearly visible. Fig. 4(b) shows the corresponding SADP of the CRA specimen. Comparing this SADP with the SADP in Fig. 3(b), one can see that the SADP of the CRA specimen exhibits near-continuous diffraction rings which are different with the discrete diffraction spots of the ST specimen. This indicates that the present cold rolling plus annealing process can give rise to significant grain refinement, and high-density grain boundaries are introduced in the CRA Ti-3014 specimen. Based on the SADP in Fig. 4(b), the nanometer-scale precipitates distributed in β matrix are determined as α phase. Additionally, there were no extra diffraction rings arising from α″ phase in Fig. 4(b), thereby indicating that the transformation from β phase to α″ martensite no longer occurred during the water quenching process after annealing. Namely, the martensitic transformation in the Ti-3014 alloy is remarkably retarded by the cold rolling plus annealing treatment. Recent studies revealed that the microstructure factors, such as dislocation and grain refinement, can play a significant influence in suppressing martensitic transformation due to the shear nature of the transformation [14,17,18]. As shown in Fig. 4, there do exist large quantities of dislocation tangles and grain boundaries in the CRA Ti-3014 alloy. Therefore, we can reasonably ascribe the retard of martensitic transformation in the CRA specimen to the microstructure factors, i.e.

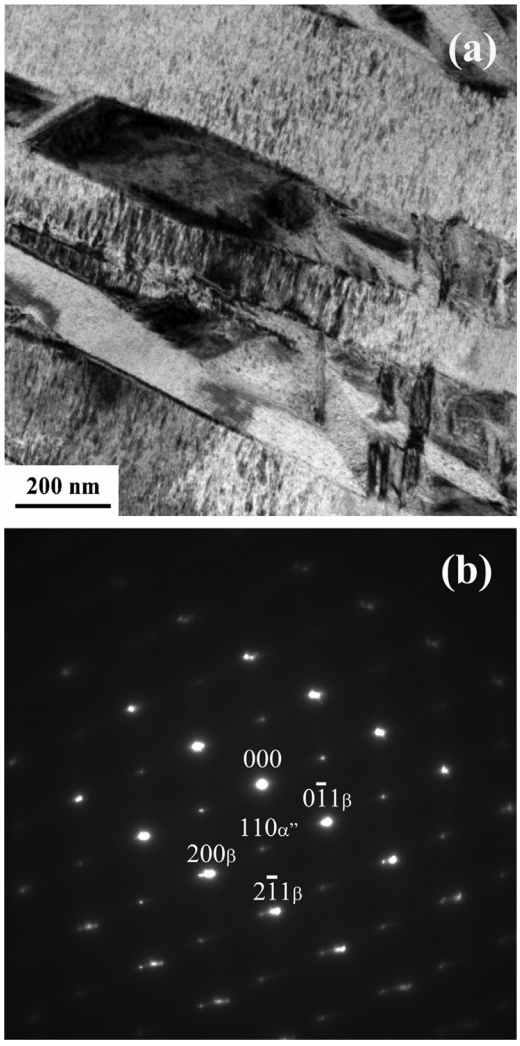

Fig. 3. A typical bright-field micrograph (a) and the corresponding [110]β zone axis selected area diffraction pattern (SADP) (b) of ST Ti-3014 specimen.

dislocation tangles and grain refinement, induced by the cold rolling plus annealing process.

Commonly, the amount of β-stabilizers in α precipitates is lower than that in β phase of the same Ti alloy [21,22]. As a result, the precipitation of α within β phase, especially for high-temperature and/or long-time annealing, may lead to an enrichment of β-stabilizers in residual β matrix [21,22]. If so, this may have an adverse effect on lowering the elastic modulus of β phase, because the elastic modulus of β increases monotonically with increasing the content of β-stabilizers [11–13]. Thus, it is quite necessary to clarify the impact of the precipitation of α on the composition of the residual β. Fig. 5 presents the EDS line scanning results of a typical area (marked with a white line in Fig. 4) covering β and α phases in the CRA specimen. It can be seen that there was no visible composition variation along the composition profiles for Ti, Nb, Mo and Sn elements, indicating that the precipitation of fine α phase did not lead to obvious composition change in residual β matrix. In other words, during the annealing at low temperature for short time (i.e., 625 K for 30 min), the partitioning of β-stabilizers between α and β phases did not occur and the amount of β-stabilizers in the residual β

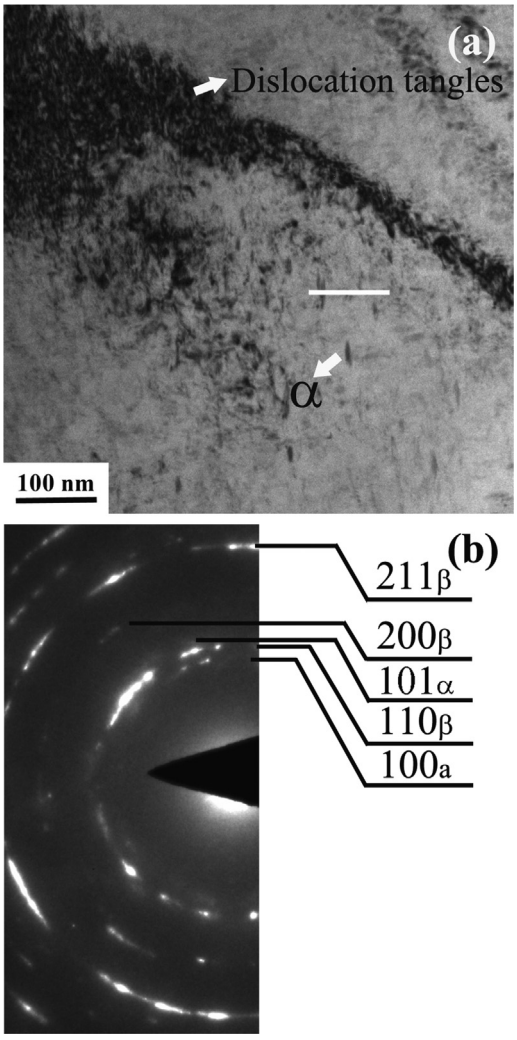

Fig. 4. Bright-field micrograph (a) and the corresponding selected area diffraction pattern (SADP) (b) of CRA Ti-3014 specimen.

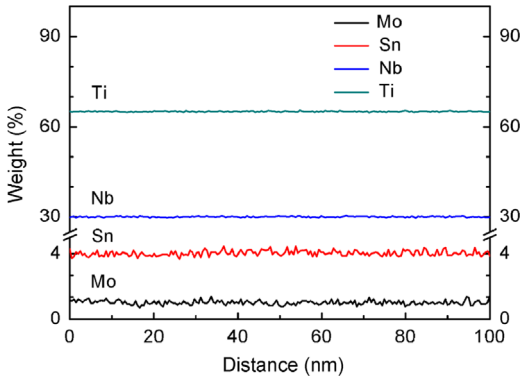

Fig. 5. EDS line scanning results of a typical area (marked with a white line in Fig. 4) covering β and α phases in the CRA Ti-3014 specimen.

phase remained at a low level. This result is consistent with a recent study on the β-type Ti-5553 alloy, where the initial small-sized α precipitates were found to be formed by a displacive transformation mode, rather than diffusional mechanism [23]. According to the results in Fig. 5, it is reasonable to expect that

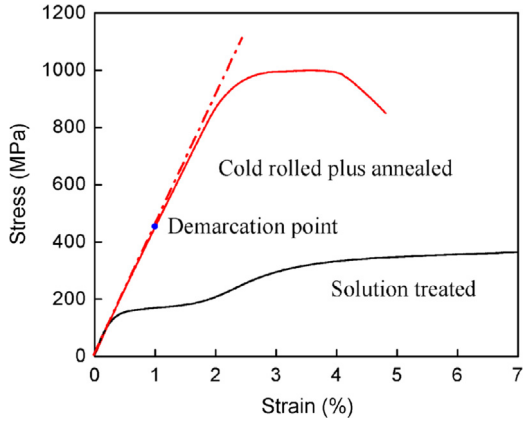

Fig. 6. Tensile stress–strain curves of ST and CRA Ti-3014 specimens.

the residual β matrix in the CRA specimen may exhibit a low elastic modulus due to its low amount of β-stabilizers.

Fig. 6 shows the tensile stress–strain curves of ST and CRA Ti-3014 specimens. The ST specimen performs typical "double yielding" behavior, characterized by the existence of stress-plateau, which is similar to that observed in the solution treated metastable β-type Ti alloys, such as Ti–Nb [24], Ti–Ta [25], and Ti–Nb–Ta–Zr alloys [26]. It has been confirmed that the presence of stress-plateau is closely related to the stress-induced α″ martensitic transformation and the reorientation of the martensite variants [24–26]. Clearly, although the ST alloy exhibits a low elastic modulus of 46 GPa, it is not the appropriate candidate for biomedical applications due to its low yield strength (~130 MPa). Interestingly, upon cold rolling plus annealing treatment, the Ti-3014 alloy was remarkably strengthened, with a yield strength of ~954 MPa and a ultimate tensile strength of ~1000 MPa. This strengthening effect can be attributed to the interaction between nanometer-scale α precipitates and high-density dislocations in the CRA specimen, as show in Fig. 4. It should be noted that in addition to high strength, the CRA specimen also exhibited an ultralow elastic modulus of 45 GPa. This level of elastic modulus is lower than that of most of β-type Ti alloys for biomedical applications [1,4,6,10]. According to the EDS results shown in Fig. 5, it is believed that the ultralow elastic modulus of the CRA specimen is mainly attributed to the ultralow modulus of β matrix caused by its low β-stabilizers content.

Referring to the stress–strain curve of CRA specimen in Fig. 6, one can also see that there exists a demarcation point, which divides the stress–strain curve into two stages, at about 1% strain. The first stage exhibits linear deformation obeying a straight line, while the second stage performs nonlinear deformation deviating from a straight line. In order to elucidate the deformation mechanism of the CRA alloy, in-situ synchrotron X-ray diffraction was conducted on the CRA specimen. Fig. 7 shows the diffraction patterns for the 110_{β} and $002_{\alpha''}$ perpendicular to the tensile direction during loading. The first pattern was detected before loading (at a strain of 0%), and the other patterns were detected by stretching the specimen at a strain interval of 0.2%, until the strain reached to 2%. It can be seen from Fig. 7 that at the initial linear deformation stage (for strain $<1\%$), only the 110_{β} peak was detected and the d-spacing of 110_{β} increased with

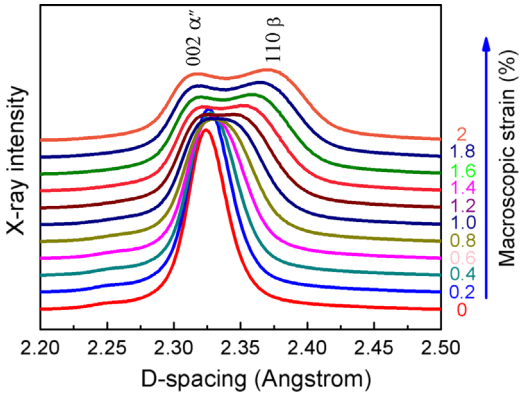

Fig. 7. In situ synchrotron X-ray diffraction patterns for the CRA 110_{β} and $002_{\alpha''}$ perpendicular to the tensile direction during loading.

increasing strain. This suggests that for when the strain is less than 1%, no stress-induced transformation occurs in the CRA specimen and the specimen exhibits elastic deformation. When the strain reaches 1%, the 110_{β} peak begins to split, and a new diffraction peak attributable to $002_{\alpha''}$ is detected in the diffraction pattern. With further increasing strain (for $1\% < \text{strain} \leq 2\%$), the intensity of 110_{β} peak decreased, while the intensity of $002_{\alpha''}$ peaks increased, indicating that the stress-induced martensitic transformation from β to α″ takes place during loading. Consequently, a demarcation point is observed in the tensile stress–strain curve of the CRA specimen due to the occurrence of stress-induced α″ martensitic transformation.

4. Conclusions

In summary, a metastable β-type Ti–30Nb–1Mo–4Sn alloy with ultralow elastic modulus and high strength was fabricated. Although the alloy exhibits low yielding stress in its solution state owing to the presence of coarse α″ martensitic laths, cold rolling plus annealing treatment can result in the combination of high yield stress of 1000 MPa and low elastic modulus of 45 GPa. The result of the present study indicates that the high-density grain boundaries and the dislocations induced by thermo-mechanical treatment retard the β→α″ martensitic transformation in Ti–30Nb–1Mo–4Sn alloy with low β-stabilizer content, and hence give rise to the ultralow elastic modulus and high tensile strength.

Acknowledgments

The authors greatly appreciate the financial support from the National Natural Science Foundation of China (51401088 and 51471017), the China Postdoctoral Science Foundation (2014M561580), the Natural Science Foundation of Jiangsu Province (BK20140549), the Natural Science Fund for Colleges and Universities in Jiangsu Province (14KJB430007), the Jiangsu Postdoctoral Science Foundation (1401107C) and the Senior Intellectuals Fund of Jiangsu University (13JDG098). The use of the Advanced Photon Source was supported by the US Department of Energy, Office of Science, and Office of Basic Energy Science, under Contract no. DE-AC02-06CH11357.

References

[1] M. Geetha, A.K. Singh, R. Asokamani, A.K. Gogia, Prog. Mater. Sci. 54 (2008) 397–425.
[2] Y.L. Hao, S.J. Li, S.Y. Sun, C.Y. Zheng, R. Yang, Acta Biomater. 3 (2007) 277–286.
[3] S. Guo, Q.K. Meng, X.N. Cheng, X.Q. Zhao, Mater. Lett. 133 (2014) 236–239.
[4] M.J. Long, H.J. Rack, Biomaterials 19 (1998) 1621–1639.
[5] W.F. Ho, C.P. Ju, J.H. Chern, Biomaterials 20 (1999) 2115–2122.
[6] H.J. Rack, J.I. Qazi, Mater. Sci. Eng. C 26 (2006) 1269–1277.
[7] Y.L. Zhou, M. Niinomi, T. Akahori, Mater. Sci. Eng. A 37 (2004) 1283–1290.
[8] S. Kuramoto, T. Furuta, J.H. Hwang, K. Nishino, T. Saito, Metall. Mater. Trans. A 37 (2006) 657–662.
[9] D. Kuroda, M. Niinomi, M. Morinaga, Y. Kato, T. Yashiro, Mater. Sci. Eng. A 243 (1998) 244–249.
[10] D. Banerjee, J.C. Williams, Acta Mater. 61 (2013) 844–879.
[11] L.M. Elias, S.G. Schneider, S. Schneider, H.M. Silva, F. Malvisi, Mater. Sci. Eng. A 43 (2006) 2108–2112.
[12] M. Tane, S. Akita, T. Nakano, K. Hagihara, Y. Umakoshi, M. Niinomi, H. Nakajima, Acta Mater. 56 (2008) 2856–2863.
[13] M. Abdel-Hady, K. Hinoshita, M. Morinaga, Scr. Mater. 55 (2006) 477–480.
[14] W. Xu, K.B. Kim, J. Das, M. Calin, B. Rellinghaus, J. Eckert, Appl. Phys. Lett. 89 (2006) 031906.
[15] H.Y. Kim, S. Hashimoto, J.I. Kim, T. Inamura, H. Hosoda, S. Miyazaki, Mater. Sci. Eng. C 417 (2006) 120–128.
[16] Y.L. Hao, S.J. Li, S.Y. Sun, R. Yang, Mater. Sci. Eng. A 441 (2006) 112–118.
[17] Y.L. Hao, M. Niinomi, D. Kuroda, K. Fukunaga, Y.L. Zhou, R. Yang, A. Suzuki, Metall. Mater. Trans. A 33 (2002) 3137–3144.
[18] H. Matsumoto, S. Watanabe, S. Hanada, J. Alloy. Compd. 439 (2007) 146–155.
[19] Y.L. Zhou, M. Niinomi, T. Aakahori, Mater. Sci. Eng. A 384 (2004) 92–101.
[20] Q.H. Guo, Y.Z. Zhan, H.L. Mo, G.H. Zhan, Mater. Des. 31 (2010) 4842–4846.
[21] Y. Al-Zain, H.Y. Kim, T. Koyano, H. Hosoda, T.H. Nam, S. Miyazaki, Acta Mater. 59 (2011) 1464–1473.
[22] O.M. Ivasishin, P.E. Markovsky, S.L. Semiatin, C.H. Ward, Mater. Sci. Eng. A 405 (2005) 296–305.
[23] S. Nag, R. Banerjee, R. Srinivasan, J.Y. Hwang, M. Harper, H.L. Fraser, Acta Mater. 57 (2009) 2136–2147.
[24] H.Y. Kim, H. Satoru, J.I. Kim, H. Hosoda, S. Miyazaki, Mater. Trans. 45 (2004) 2443–2448.
[25] P.J. Buenconsejo, Y.H. Kim, H. Hosoda, S. Miyazaki, Acta Mater. 57 (2009) 1068–1077.
[26] S. Nobuhito, N. Mitsuo, A. Toshikazu, T. Junji, T. Hiroyuki, Mater. Sci. Eng. C 25 (2005) 363–369.